Influence of axial mass and strange axial form factor on neutrino-nucleus scattering in the quasielastic region

K. S. Kim*
School of Liberal Arts and Science, Korea Aerospace University, Koyang 412-791, Korea

Hungchong Kim
Department of General Education, Kookmin University, Seoul 136-702, Korea

Myung-Ki Cheoun and Ghil-Seok Yang
Department of Physics, Soongsil University, Seoul 156-743, Korea

W. Y. So
Department of Radiological Science, Kangwon National University, Samcheok 245-711, Korea
(Received 28 May 2015; revised manuscript received 31 August 2015; published 20 October 2015)

We study the effects of the strange axial form factor and axial mass on both neutral- and charged-current reactions in the quasielastic region within the framework of a relativistic single-particle model. For this purpose, we calculate the differential cross section, the separated cross sections associated with the longitudinal and transverse response functions, the asymmetry for the neutral-current reaction, and the various ratios of the neutral- to charged-current reactions. The calculations are performed for a ^{12}C target at specific incident neutrino (antineutrino) energies of 0.5 and 1.5 GeV, or with the flux-averaged incident energies of the MiniBooNE experiment. Then, we discuss the dependence of the cross sections, asymmetry, and ratios on the axial mass and strange axial form factor. Finally, we compare our calculations with the MiniBooNE experimental data.

DOI: 10.1103/PhysRevC.92.044613 PACS number(s): 25.30.Pt, 13.15.+g, 24.10.Jv

I. INTRODUCTION

With the recent development of neutrino-beam facilities, interest in neutrino-nucleus ($\nu - A$) scattering has increased. This scattering was widely applied in various fields of physics, such as astrophysics, cosmology, particle physics, and nuclear physics. In nuclear physics, $\nu - A$ scattering is one of the powerful tools used to study aspects of the weak interaction, such as strangeness and the axial form factor (G_A) of nucleon [1].

For example, the uncertainty regarding the strangeness content was studied using the Paschos-Wolfenstein relation [2] for a nucleon and target nuclei, and the strangeness contribution to G_A was determined within an uncertainty of 0.015. However, this value is heavily dependent on the strangeness magnetic moment and the isospin of the target nucleus [3]. Alberico *et al.* [4] have calculated the ($\nu - A$) scattering within two relativistic independent-particle models (the Fermi gas and shell models), and found that the final state interaction (FSI) significantly affects the ratio of the neutral-current (NC) to charged-current (CC) reactions at an incident neutrino energy of $E_\nu \geqslant 200$ MeV.

On the other hand, in our previous works [5], we studied the effect of the density-dependent weak form factor generated from the quark meson coupling (QMC) model for ($\nu - A$) scattering. Hence, it was found that the density effect reduces the cross section for both incident neutrinos and antineutrinos, with the effect on G_A being the largest, while that on the Dirac form factor (F_1) is very small. In addition, we investigated the effect of the FSI, and found that the FSI description may play an important role in estimation of the cross sections. Furthermore, the FSI effect on each response cross section may differ from those on the differential cross sections [6].

The MiniBooNE Collaboration has recently reported four kinds of high statistical flux-averaged differential cross-section data, i.e., for muon neutrino CC [7], neutrino NC [8], muon antineutrino CC [9], and antineutrino NC [10] scattering from CH_2 as a function of the four-momentum transfer square, $Q^2 = -q^\mu q_\mu$. In particular, new values for the axial mass (M_A) and strange axial form factor (g_A^s) from the NC reaction [8] were extracted at $Q^2 = 0$, with $M_A = 1.39 \pm 0.11$ GeV and $g_A^s = 0.08 \pm 0.26$. In particular, this M_A value deviates significantly from the previous standard value. However, intensive discussion continues as to whether such deviations stem from nuclear structure effects or the uncertainty inherent in M_A itself. The induced pseudoscalar coupling constant of the axial current deduced from the radiative muon capture [11] is a similar problem wherein it exhibits a deviation of approximately 25% from the standard value [12].

As the effects of the nuclear structure on the target were not fully determined in the MiniBooNE experiments, a large number of theoretical studies [13–17] have been devoted to this problem. For example, the authors of Ref. [13] calculated inclusive CC $\nu - A$ scattering including two-nucleon processes and π production, and they compared their results with the MiniBooNE data by scaling $M_A = 1.03$ GeV to $M_A = 1.35$ GeV. However, their results were found to yield overestimated values compared to the experimental data. Another study [14] has investigated the cross-section

*kyungsik@kau.ac.kr

dependence on M_A by changing this value from its world average value to 1.23 GeV, or even by applying an overall factor (=1.2) to a spectral function. The obtained theoretical result describes the MiniBooNE data within a relativistic Fermi gas model. In Refs. [15–17], the cross-section dependence on g_A^s as well as M_A was studied and compared with the MiniBooNE data. Using the LEA code [18], the authors of Ref. [15] extracted $M_A = 1.28 \pm 0.05$ GeV and $g_A^s = -0.11 \pm 0.36$. Furthermore, Meucci *et al.* [16] performed NC $\nu - A$ scattering calculations using a relativistic Green's function and obtained reasonable agreement with the MiniBooNE data, without increasing the standard value of M_A. However, the sensitivity to g_A^s was shown to be somewhat small, therefore g_A^s could be changed from 0.34 to -0.18 without degrading the agreement with the experimental data.

In Ref. [17], the fitted values of M_A and g_A^s were estimated by calculating the $(\nu p \to \nu p)/(\nu N \to \nu N)$ ratio and comparing the MiniBooNE data with two nuclear models, namely, the super-scaling approximation (SUSA) and relativistic mean field (RMF) models. The values extracted from the RMF and SUSA models were $(M_A, g_A^s) = (1.34 \pm 0.06\ \text{GeV}, 0.04 \pm 0.28)$ and $(1.42 \pm 0.06\ \text{GeV}, -0.06 \pm 0.31)$, respectively. In our previous paper [19], we studied the influence of g_A^s. Although the effect of g_A^s on the cross section is very small, it can be distinguished from the other contributing factors by calculating the difference and summation of the asymmetries between the NC and CC reactions. However, the majority of theoretical analyses have focused on only one of the four available scattering data sets. In our previous paper [20], we suggested the combination of some physical observables with the accumulated scattering data. For example, NC-to-CC ratios (or neutrino to antineutrino cross sections) and their asymmetries can provide valuable opportunities to study the strangeness content of nucleons and/or nuclei.

In this work, we investigate the sensitivity of such observables as well as the cross sections to M_A and g_A^s in inclusive NC and CC $\nu(\bar{\nu}) - A$ scattering from a ^{12}C target. To calculate these reactions, we use a relativistic single-particle model that requires bound-state and continuum-nucleon wave functions and a transition current operator. The bound-nucleon wave functions are solutions to the Dirac equation in the presence of the strong scalar and vector potentials of the $\sigma - \omega$ model [21]. The wave functions of the knocked-out nucleons are generated by the same bound-nucleon potential, called the RMF. This RMF model guarantees the current conservation and gauge invariance. This model provides a very good description of (e,e') Bates experimental data with good treatment of Coulomb distortion for the incoming and outgoing electrons [22]. In particular, to include the Coulomb distortion of the outgoing leptons, we use the same method as in our previous work [23].

The outline of this paper is as follows: In Sec. II, we briefly present the formalism for the NC and CC reactions; in Sec. III, our numerical results for the cross sections, separated cross sections, ratios, and asymmetry of the corresponding cross sections are presented; and in Sec. IV, the summary and conclusion are given.

II. FORMALISM

To model the $\nu(\bar{\nu}) - A$ scattering mathematically, we choose the nucleus rest frame where the target nucleus is positioned at the origin of the coordinate system. The four-momenta of the incoming and outgoing neutrinos (antineutrinos) are labeled $p_i^\mu = (E_i, \mathbf{p}_i)$ and $p_f^\mu = (E_f, \mathbf{p}_f)$. $p_A^\mu = (E_A, \mathbf{p}_A)$, $p_{A-1}^\mu = (E_{A-1}, \mathbf{p}_{A-1})$, and $p^\mu = (E_N, \mathbf{p})$ represent the four-momenta of the target nucleus, the residual nucleus, and the knocked-out nucleon, respectively. In the laboratory frame, the inclusive cross section for the NC and CC reactions is given by the contraction between the lepton and hadron tensor,

$$\frac{d\sigma}{dT_N} = 4\pi^2 \frac{M_N M_{A-1}}{(2\pi)^3 M_A} \int \sin\theta_l d\theta_l \int \sin\theta_N d\theta_N\, p f_{rec}^{-1} \sigma_M^{Z,\,W^\pm} \times [v_L R_L + v_T R_T + h v_T' R_T'], \tag{1}$$

where θ_l denotes the scattering angle of the lepton, θ_N is the polar angle of the knocked-out nucleons, and $h = -1$ ($h = +1$) corresponds to the helicity of the incident ν ($\bar{\nu}$). The R_L, R_T, and R_T' terms are the longitudinal, transverse, transverse-interference response functions, respectively. The squared four-momentum transfer is given by $Q^2 = q^2 - \omega^2 = -q_\mu^2$. For the NC reaction, the kinematic factor (σ_M^Z) is defined by

$$\sigma_M^Z = \left(\frac{G_F \cos(\theta_l/2) E_f M_Z^2}{\sqrt{2}\pi \left(Q^2 + M_Z^2\right)} \right)^2, \tag{2}$$

and for the CC reaction,

$$\sigma_M^{W^\pm} = \sqrt{1 - \frac{M_l^2}{E_f^2}} \left(\frac{G_F \cos(\theta_C) E_f M_W^2}{2\pi \left(Q^2 + M_W^2\right)} \right)^2, \tag{3}$$

where M_Z and M_W are the rest masses of the Z and W bosons, respectively. θ_C represents the Cabibbo angle given by $\cos^2\theta_C \simeq 0.9749$. The recoil factor ($f_{\text{rec}}$) is expressed as

$$f_{\text{rec}} = \frac{E_{A-1}}{M_A} \left| 1 + \frac{E_p}{E_{A-1}} \left[1 - \frac{\mathbf{q}\cdot\mathbf{p}}{p^2} \right] \right|. \tag{4}$$

For both NC and CC reactions, explicit expressions for the kinematical coefficients v_L, v_T, and v_T' and the corresponding response functions R_L, R_T, and R_T' in Eq. (1) can be found in Ref. [19].

The weak current (J^μ) represents the Fourier transform of the nucleon current density, which is expressed as

$$J^\mu = \int \bar{\psi}_p \hat{\mathbf{J}}^\mu \psi_b e^{i\mathbf{q}\cdot\mathbf{r}} d^3r, \tag{5}$$

where $\hat{\mathbf{J}}^\mu$ is a free weak nucleon current operator and ψ_p and ψ_b are wave functions of the knocked-out and bound-state nucleons, respectively. For a free nucleon, the current operator comprises the weak vector and the axial vector form factors,

$$\hat{\mathbf{J}}^\mu = F_1^V(Q^2)\gamma^\mu + F_2^V(Q^2)\frac{i}{2M_N}\sigma^{\mu\nu}q_\nu + G_A(Q^2)\gamma^\mu\gamma^5 + \frac{1}{2M_N} G_P(Q^2) q^\mu \gamma^5, \tag{6}$$

where M_N denotes the nucleon mass. By the conservation of the vector current (CVC) hypothesis, the vector form factors for the proton (neutron) $[F_i^{V,p(n)}(Q^2)]$ are expressed as

$$F_i^{V,p(n)}(Q^2) = \left(\frac{1}{2} - 2\sin^2\theta_W\right)F_i^{p(n)}(Q^2) - \frac{1}{2}F_i^{n(p)}(Q^2) - \frac{1}{2}F_i^s(Q^2), \quad \text{for the NC},$$
$$F_i^V(Q^2) = F_i^p(Q^2) - F_i^n(Q^2), \quad \text{for the CC}, \tag{7}$$

where θ_W is the Weinberg angle given by $\sin^2\theta_W = 0.2224$.

The strange vector form factor $[F_i^s(Q^2)]$ in Eq. (7) is usually given in dipole form, independently of the nucleon isospin, such that

$$F_1^s(Q^2) = \frac{F_1^s(0)Q^2}{(1+\tau)\left(1+Q^2/M_V^2\right)^2},$$
$$F_2^s(Q^2) = \frac{F_2^s(0)}{(1+\tau)\left(1+Q^2/M_V^2\right)^2}, \tag{8}$$

where $\tau = Q^2/(4M_N^2)$ and $M_V = 0.843$ GeV is the cut-off mass parameter usually adopted for nucleon electromagnetic form factors. $F_1^s(0)$ is defined as $F_1^s(0) = dG_E^s(Q^2)/dQ^2|_{Q^2=0} = 0.53\ \text{GeV}^{-2}$ and $F_2^s(0) = \mu_s = -0.4$ is an anomalous strange magnetic moment.

The axial form factors are given by

$$G_A(Q^2) = \frac{1}{2}\left(\mp g_A + g_A^s\right)/\left(1+Q^2/M_A^2\right)^2, \tag{9}$$

where $g_A = 1.262$. As we have stated in the introduction, the main purpose of this work is to investigate the cross-section sensitivity to these parameters. The $-(+)$ signs are from the isospin dependence, and correspond to the knocked-out proton (neutron).

The induced pseudoscalar form factor is parametrized by the Goldberger-Treimann relation,

$$G_P(Q^2) = \frac{2M_N}{Q^2+m_\pi^2}G_A(Q^2), \tag{10}$$

where m_π is the pion mass. However, note that the contribution of the pseudoscalar form factor vanishes for the NC reaction, because of the negligible final lepton mass participating in this reaction.

III. RESULTS

Within the framework of a relativistic single-particle model, we investigate the effects of M_A and g_A^s on the weak current. The bound-nucleon wave functions are solutions to the Dirac equation in the presence of the strong scalar and vector potentials of the $\sigma-\omega$ model [21]. For the FSI, the wave functions of the knocked-out nucleons are obtained by solving a Dirac equation with the same potential as the bound nucleons, which is referred to as the RMF. For the CC reaction, the Coulomb distortion of the outgoing leptons is an important component. Hence, we use the approximate distorted-wave Born approximation (DWBA) generated by the Ohio University group [22].

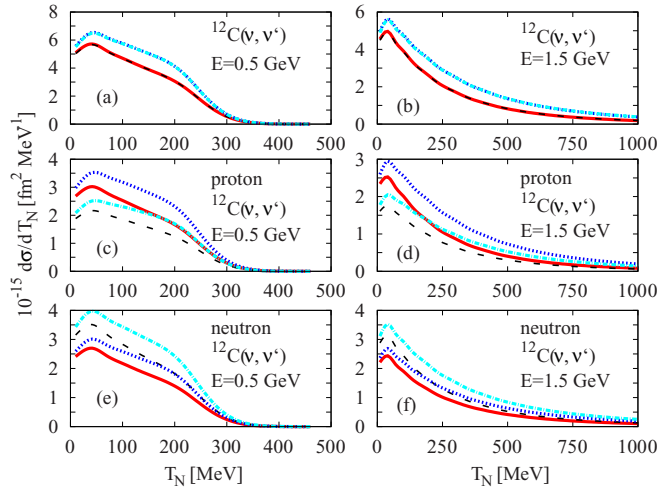

FIG. 1. (Color online) Differential cross sections of NC $\nu - A$ scattering in terms of knocked-out nucleon kinetic energy for 0.5- (left panel) and 1.5-GeV (right panel) incident neutrino energies from ^{12}C. The solid (red) curves are the results for $M_A = 1.032$ GeV and $g_A^s = -0.19$, the dashed (black) curves are for $M_A = 1.032$ GeV and $g_A^s = 0.08$, the dotted (blue) curves are for $M_A = 1.39$ GeV and $g_A^s = -0.19$, and the dash-dot-dotted (sky-blue) curves are for $M_A = 1.39$ GeV and $g_A^s = 0.08$. (a) and (b) Sums of proton and neutron knockouts. (c) and (d) Cross sections for proton knockout. (e) and (f) Cross sections for neutron knockout.

A. Cross section

As shown in Fig. 1, to determine the dependence of M_A and g_A^s on the neutrino-scattering cross sections, we present the differential cross sections for the NC reaction of the ^{12}C nucleus in terms of the kinetic energies of the knocked-out nucleons for four different conditions: $(M_A, g_A^s) = (1.032, -0.19), (1.032, 0.08), (1.39, -0.19)$, and $(1.39, 0.08)$. Cross sections with incident neutrino energy of $E = 0.5$ and 1.5 GeV are shown in the left and right panels, respectively. In each figure, the solid (red) curves are the results for $M_A = 1.032$ GeV and $g_A^s = -0.19$, the dashed (black) curves are for $M_A = 1.032$ GeV and $g_A^s = 0.08$, the dotted (blue) curves are for $M_A = 1.39$ GeV and $g_A^s = -0.19$, and the dash-dot-dotted (sky-blue) curves are for $M_A = 1.39$ GeV and $g_A^s = 0.08$. Figures 1(a) and 1(b) show the sums of the proton and neutron knockouts. Figures 1(c) and 1(d) show proton knockout results, while Figs. 1(e) and 1(f) show the neutron knockout data.

The g_A^s contribution has a different effect on the proton and neutron knockouts. Changing g_A^s from -0.19 to 0.08 reduces the cross section for the former but increases that of the latter. As a result, the g_A^s contribution to the sum of the cross sections is very small, as can be seen in Figs. 1(a) and 1(b). On the other hand, the contribution of M_A is somewhat noticeable in both cases. A larger value of M_A increases both cross sections, but the sensitivity of the proton knockouts is slightly higher.

Figure 2 shows that the incident antineutrino cross sections and kinematics are the same as in Fig. 1. The shapes are similar to those of Fig. 1, but the cross-section magnitudes are smaller than those for the neutrino case. We also obtain

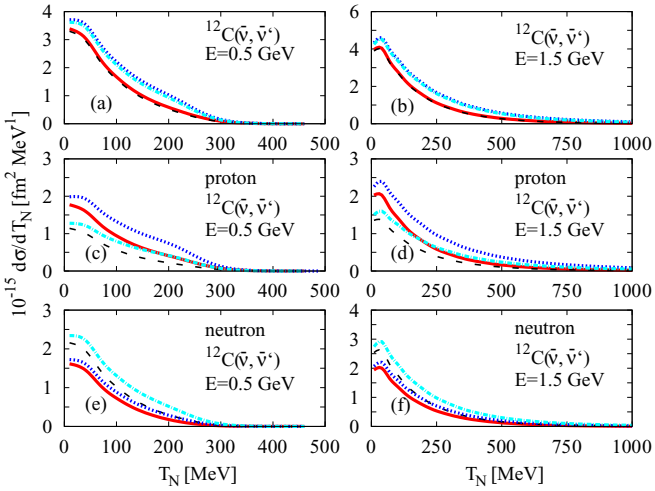

FIG. 2. (Color online) Identical to Fig. 1, but for antineutrinos.

similar cross-section sensitivity to g_A^s and M_A to that of the neutrino scattering case. Therefore, the cross sections of both the $^{12}C(\nu,\nu')$ and $^{12}C(\bar{\nu},\bar{\nu}')$ reactions are almost independent of g_A^s, because the effects are canceled out by the neutrons and protons. However, these cross sections depend on M_A.

The energy of the incoming neutrinos is not fixed in actual neutrino experiments. Instead, the incoming neutrinos have an energy spectrum and the associated cross sections must be averaged over the flux. To confirm that M_A and g_A^s play the same roles in actual experiments, we also calculate the flux-averaged differential cross section using the neutrino spectrum for MiniBooNE experiments. In Fig. 3, we show the flux-averaged differential cross sections per nucleon for the NC reaction in terms of Q^2. The left and right panels show the neutrino and antineutrino results, respectively. The neutrino and antineutrino experimental data were measured at MiniBooNE (Refs. [8] and [10], respectively). Qualitatively,

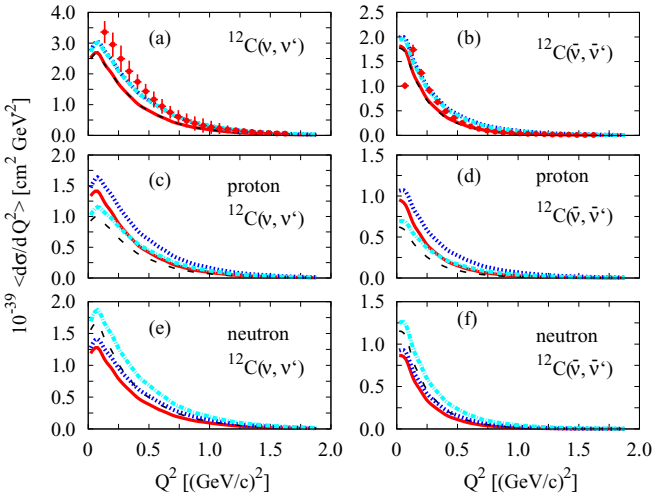

FIG. 3. (Color online) Flux-averaged differential cross sections ($\langle d\sigma/dQ^2\rangle$) per nucleon for $\nu N \to \nu N$ and $\bar{\nu}N \to \bar{\nu}N$. The curves are defined as in Fig. 1. The neutrino and antineutrino experimental data were measured at MiniBooNE (Refs. [8] and [10], respectively).

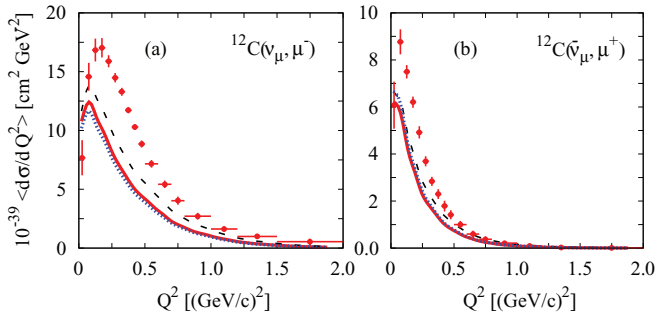

FIG. 4. (Color online) Flux-averaged differential cross sections for CC reaction. The solid curves are the results of $M_A = 1.032$ GeV and the dashed lines are for $M_A = 1.39$ MeV. The dotted (blue) curves are the results without Coulomb distortion of the final lepton with $M_A = 1.032$ GeV. The neutrino and antineutrino experimental data were measured at MiniBooNE (Refs. [7] and [9], respectively).

we obtain similar sensitivity to g_A^s and M_A as that seen in Figs. 1 and 2.

In Fig. 4, the flux-averaged differential cross sections per nucleon for the CC reaction are presented in terms of Q^2. The neutrino and antineutrino experimental data were measured at MiniBooNE (Refs. [7] and [9], respectively). In the case of the CC reaction, as this is an isovector interaction, the isoscalar-type interaction represented by g_A^s does not contribute to the cross section. Thus, from the CC reaction, we can examine the cross section as we vary M_A only, from $M_A = 1.032$ to 1.39 GeV. The cross section increases by approximately 15% with larger values of M_A, as before. For both incident neutrinos [$^{12}C(\nu_\mu,\mu^-)$] and antineutrinos [$^{12}C(\bar{\nu}_\mu,\mu^+)$], our theoretical results (solid lines) are lower than the data, by approximately 35% in the vicinity of the peak. This disagreement was also observed in the total cross sections and double differential cross sections of CC scattering [5]. In Fig. 4, the dotted (blue) curves are the results obtained without considering the Coulomb distortion of the final lepton for $M_A = 1.032$ GeV. The Coulomb distortion increases (decreases) the flux-averaged differential cross sections for the neutrino (antineutrino) case. However, the changed amounts in both cross sections are so small as to be negligible, as the ^{12}C target is a light nucleus and the projectile particles have no charge, contrary to the case of electron scattering. These results are identical to those of our previous work [23].

B. Response cross sections

To investigate the cross-section dependence on M_A and g_A^s in more detail, we study the response cross sections, which are defined as the cross sections connected to R_L, R_T, and R_T', as shown in Eq. (1). In Fig. 5, we show the flux-averaged cross sections of each response function, which integrate over the scattering angle and the polar angle of the knocked-out nucleon in Eq. (1) as a function of Q^2. The left and right panels show the proton and neutron results, respectively. The curves are defined as in Fig. 1. In the proton case, the longitudinal cross section is most sensitive to g_A^s. Here, g_A^s reduces all the response cross sections, but M_A increases them. Note that the sensitivity to M_A is similar for all the response cross sections. In the neutron

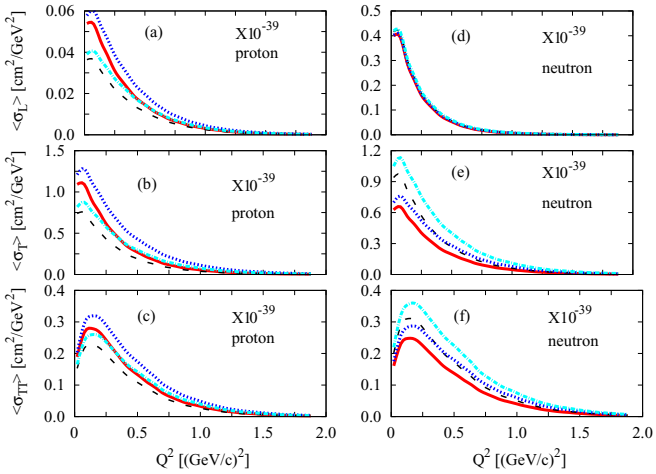

FIG. 5. (Color online) Response cross sections for NC flux-averaged differential cross sections.

case, the longitudinal cross section is almost insensitive to both M_A and g_A^s, but the other response functions increase in accordance with increasing M_A and g_A^s. The response cross sections have similar shapes, and the main contribution to the differential cross section is from the transverse response cross section. However, similar to the differential cross sections in Sec. III A, summation over the protons and neutrons for each response term does not yield any discernible g_A^s dependence.

In Fig. 6, the response cross sections for the CC reactions are shown. M_A increases the response cross sections, but the sensitivity of the longitudinal response to M_A is very small. All three response cross sections have the same shape, and the magnitudes in the neutrino case are larger than those in the antineutrino case. The magnitude of the transverse response cross section is dominant, as in Fig. 5.

C. Asymmetry and ratios

In this subsection, we study the asymmetry of the NC reaction and the various ratios of the NC-to-CC reactions.

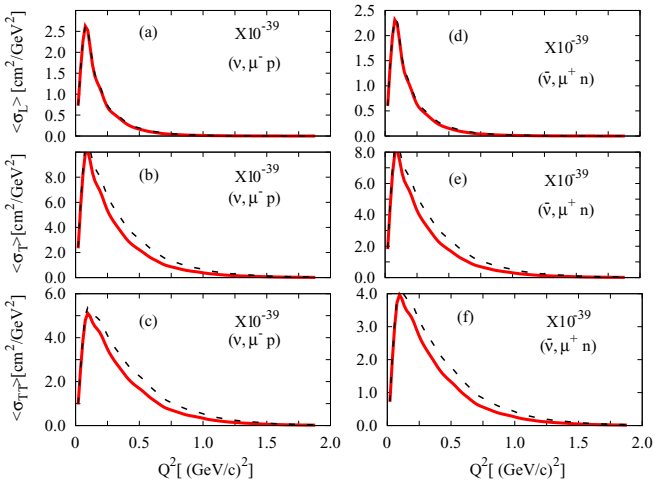

FIG. 6. (Color online) Identical to Fig. 5, but for CC reaction.

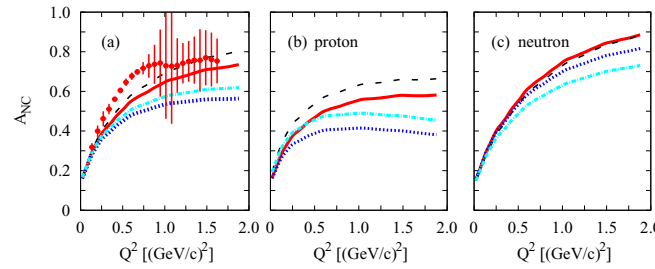

FIG. 7. (Color online) Asymmetry of flux-averaged differential cross sections for NC reaction. The data were measured at MiniBooNE [8,10]. The curves are defined as in Fig. 1.

First, the asymmetry is defined as

$$A_{\rm NC} = \frac{\sigma(\nu) - \sigma(\bar{\nu})}{\sigma(\nu) + \sigma(\bar{\nu})}, \tag{11}$$

where $\sigma(\nu)$ and $\sigma(\bar{\nu})$ denote the neutrino and antineutrino differential cross sections in Eq. (1), respectively. In particular, $A_{\rm NC}$ is sensitive to the axial current, because the nominator contains only the axial current term and the nuclear structure effects may be canceled out [20].

Figure 7 shows the asymmetry of the flux-averaged differential cross sections for the NC reaction. The data were measured at MiniBooNE [8,10] and the curves are defined as in Fig. 1. The sensitivity of the asymmetry to g_A^s and M_A differs for the various flux-averaged differential cross sections. For the protons, g_A^s and M_A enhance and reduce the asymmetry, respectively. However, in the neutron case, both g_A^s and M_A reduce the asymmetry. This means that the present asymmetry result favors larger g_A^s and lower M_A. However, it should be noted that our theoretical asymmetry does not provide a good description of the MiniBooNE data in low-Q^2 regions, because our incident neutrino cross section underestimates the data by approximately 20%. A more detailed nuclear model and more thorough descriptions of neutrino scattering are necessary to yield a final conclusion on the g_A^s dependence.

We introduce various NC-to-CC reaction ratios:

$$R_{\rm NC/CC} = \frac{\sigma_{\rm NC}(\nu,\nu'\,p)}{\sigma_{\rm CC}(\bar{\nu},\mu^+\,n)}, \qquad \text{(a)}$$

$$\text{or} = \frac{\sigma_{\rm NC}(\nu,\nu'\,n)}{\sigma_{\rm CC}(\nu,\mu^-\,p)}, \qquad \text{(b)}$$

$$\text{or} = \frac{\sigma_{\rm NC}(\nu,\nu'\,p)}{\sigma_{\rm CC}(\nu,\mu^-\,p)}, \qquad \text{(c)}$$

$$\text{or} = \frac{\sigma_{\rm NC}(\nu,\nu'\,n)}{\sigma_{\rm CC}(\bar{\nu},\mu^+\,n)}. \qquad \text{(d)} \tag{12}$$

These ratios are focused on the incident neutrinos of the NC reaction and can be used to study the effect of M_A, because the CC reaction does not contain g_A^s.

In Fig. 8, we show the NC-to-CC reaction ratios using the flux-averaged differential cross sections. The solid (red) and dashed (black) lines are the results for $M_A = 1.032$ and 1.39 GeV, respectively. Note that we use $g_A^s = -0.19$. Figures 8(a)–8(d) correspond to Eqs. (12a)–(12d), respectively. The sensitivity to M_A increases with higher Q^2. At the ratio given in Eq. (12b), the M_A dependence is very

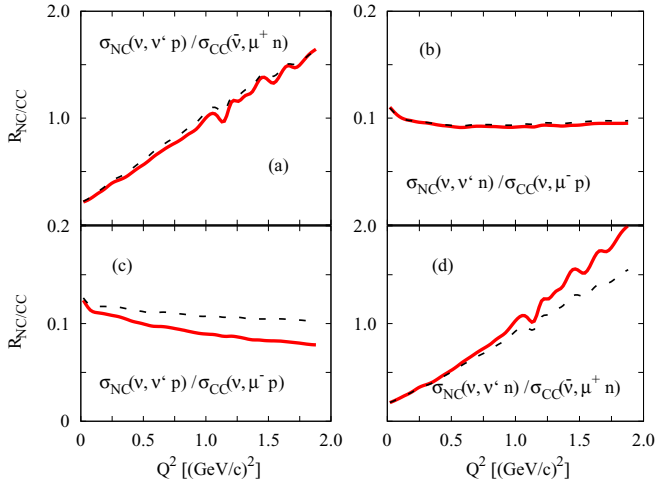

FIG. 8. (Color online) NC-to-CC reaction ratios for neutrinos in the NC reaction. The solid (red) and dashed (black) lines are the results for $M_A = 1.032$ and 1.39 GeV, respectively.

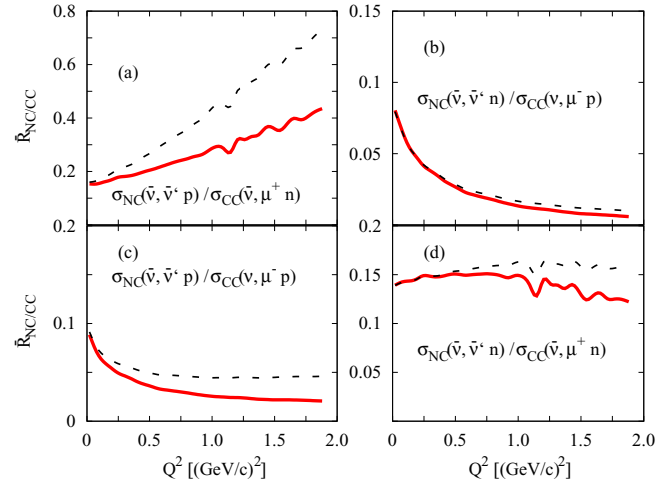

FIG. 9. (Color online) NC-to-CC reaction ratios for antineutrinos in the NC reaction. The solid (red) and dashed (black) lines are the results for $M_A = 1.032$ and 1.39 GeV, respectively.

small, where the target nucleons for both the numerator and denominator are neutrons. The finding that the NC-to-CC ratio in the neutron case is insensitive to the M_A value is slightly surprising.

As an alternative approach, we introduce other NC-to-CC reaction ratios:

$$\bar{R}_{\mathrm{NC/CC}} = \frac{\sigma_{\mathrm{NC}}(\bar{\nu},\bar{\nu}'\ p)}{\sigma_{\mathrm{CC}}(\bar{\nu},\mu^+\ n)}, \qquad \text{(a)}$$

$$\text{or} = \frac{\sigma_{\mathrm{NC}}(\bar{\nu},\bar{\nu}'\ n)}{\sigma_{\mathrm{CC}}(\nu,\mu^-\ p)}, \qquad \text{(b)}$$

$$\text{or} = \frac{\sigma_{\mathrm{NC}}(\bar{\nu},\bar{\nu}'\ p)}{\sigma_{\mathrm{CC}}(\nu,\mu^-\ p)}, \qquad \text{(c)}$$

$$\text{or} = \frac{\sigma_{\mathrm{NC}}(\bar{\nu},\bar{\nu}'\ n)}{\sigma_{\mathrm{CC}}(\bar{\nu},\mu^+\ n)}. \qquad \text{(d)} \qquad (13)$$

Note that Eq. (13) focuses on the incident antineutrinos of the NC reaction.

Figure 9 shows the ratios given in Eq. (13) for the antineutrinos of the NC reaction. The curves are defined as in Fig. 8. The effect of M_A on the knocked-out protons in the NC reaction is much larger than that for the knocked-out neutrons. As in Fig. 8, the M_A dependence for Eq. (13b) is very small, where the target nucleons for both the numerator and denominator are neutrons. The effect increases with higher Q^2.

To compare these ratios to available experimental data, we calculate other inclusive NC-to-CC reaction ratios, as shown in Fig. 10. The cross sections used here are the results given in Figs. 3 and 4. The left and right panels show the results for incident neutrinos and antineutrinos, respectively, in both the numerator and denominator. The solid curves represent the ratios for $M_A = 1.032$ GeV, the dashed lines are for $M_A = 1.39$ GeV, and the data were measured at MiniBooNE [8,10]. For both the neutrino and antineutrino cases, our results behave similarly to the experimental data. However, our values are overestimated compared to the data. Thus, the effect of M_A on the antineutrinos appears to be larger.

IV. SUMMARY

In this paper, we investigated the effects of the strange axial form factor (g_A^s) and the axial mass (M_A) on the NC and CC reactions from a ^{12}C nucleus within the framework of a relativistic single-particle model. Our theoretical results were compared with the MiniBooNE experimental data. It was shown that our results describe the NC experimental data relatively well, but they underestimate the CC data by approximately 35%.

To investigate these effects, we calculated the differential cross section, flux-averaged cross section, flux-averaged response cross sections, asymmetry, and various ratios. For both protons and neutrons, M_A increases the cross sections but reduces the asymmetry. For protons [$(\nu,\nu' p)$ scattering], g_A^s reduces the cross sections but increases the asymmetry; however, the opposite occurs for neutrons [$(\nu,\nu' n)$ scattering]. Hence, as regards the net results of the inclusive (ν,ν') scattering, the effect of g_A^s on the cross sections is minimally discernible. However, g_A^s does increase the asymmetry. It is also interesting that the neutrino scattering asymmetry favors $M_A \sim 1.03$ GeV. For the NC-to-CC reaction ratios, it is

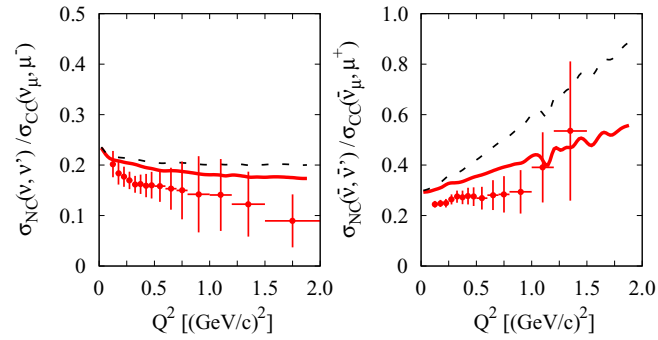

FIG. 10. (Color online) NC-to-CC reaction ratios for neutrinos and antineutrinos. The solid (red) and dashed (black) lines are the results for $M_A = 1.032$ and 1.39 GeV, respectively.

possible to study the influence of M_A on the knocked-out protons of the NC reactions distinctly.

In conclusion, the results obtained by varying M_A and examining the effects describe the MiniBooNE data for the NC reactions, but do not explain the CC-reaction MiniBooNE data at all. Further, the Coulomb distortions of outgoing leptons in the CC reactions were found to be less than a few % of the corresponding cross sections. Thus, various improvements to our current nuclear model are necessary to reproduce the MiniBooNE data. New analysis of the CC MiniBooNE data is also required.

ACKNOWLEDGMENTS

This work was supported by the National Research Foundation of Korea (Grants No. 2015R1A2A2A01004727, No. 2014R1A2A2A05003548, No. 2012M7A1A2055605, No. 2015R1D1A3A01017378, and No. 2013R1A1A2063590).

[1] O. Moreno, P. Sarriguren, E. Moya de Guerra, J. M. Udias, T. W. Donnelly, and I. Sick, Nucl. Phys. A **828**, 306 (2009).
[2] E. A. Paschos and L. Wolfenstein, Phys. Rev. D **7**, 91 (1973).
[3] C. Praet, N. Jachowicz, J. Ryckebusch, P. Vancraeyveld, and K. Vantournhout, Phys. Rev. C **74**, 065501 (2006).
[4] W. M. Alberico *et al.*, Phys. Lett. B **438**, 9 (1998).
[5] K. S. Kim, M.-K. Cheoun, and W. Y. So, Phys. Rev. C **90**, 017601 (2014); K. S. Kim, M.-K. Cheoun, W. Y. So, and H. Kim, *ibid.* **91**, 014606 (2015).
[6] K. S. Kim, M.-K. Cheoun, and W. Y. So, Phys. Rev. C **88**, 044615 (2013).
[7] A. A. Aguilar-Arevalo *et al.* (MiniBooNE Collaboration), Phys. Rev. D **81**, 092005 (2010).
[8] A. A. Aguilar-Arevalo *et al.* (MiniBooNE Collaboration), Phys. Rev. D **82**, 092005 (2010).
[9] A. A. Aguilar-Arevalo *et al.* (MiniBooNE Collaboration), Phys. Rev. D **88**, 032001 (2013).
[10] A. A. Aguilar-Arevalo *et al.* (MiniBooNE Collaboration), Phys. Rev. D **91**, 012004 (2015).
[11] G. Jonkmans *et al.* Phys. Rev. Lett. **77**, 4512 (1996).
[12] M. K. Cheoun and I.-T. Cheon, J. Phys. G **29**, 293 (2003).
[13] J. Nieves, I. R. Simo, and M. J. Vicente Vacas, Phys. Rev. C **83**, 045501 (2011).
[14] A. M. Ankowski, Phys. Rev. C **86**, 024616 (2012).
[15] A. V. Butkevich and D. Perevalov, Phys. Rev. C **84**, 015501 (2011).
[16] A. Meucci, C. Giusti, and F. D. Pacati, Phys. Rev. D **84**, 113003 (2011).
[17] R. Gonzalez-Jimenez, M. V. Ivanov, M. B. Barbaro, J. A. Caballero, and J. M. Udias, Phys. Lett. B **718**, 1471 (2013).
[18] J. J. Kelly, http://www.physics.umd.edu/enp/jjkelly/LEA.
[19] K. S. Kim, M.-K. Cheoun, and B. G. Yu, Phys. Rev. C **77**, 054604 (2008).
[20] M.-K. Cheoun and K. S. Kim, J. Phys. G **35**, 065107 (2008).
[21] C. J. Horowitz and B. D. Serot, Nucl. Phys. A **368**, 503 (1981).
[22] K. S. Kim, L. E. Wright, Y. Jin, and D. W. Kosik, Phys. Rev. C **54**, 2515 (1996); K. S. Kim, L. E. Wright, and D. A. Resler, *ibid.* **64**, 044607 (2001); K. S. Kim and L. E. Wright, *ibid.* **72**, 064607 (2005); K. S. Kim, B. G. Yu, and M. K. Cheoun, *ibid.* **74**, 067601 (2006).
[23] K. S. Kim and M.-K. Cheoun, Phys. Rev. C **83**, 034607 (2011).